Environmental Earth Sciences manuscript No.
(will be inserted by the editor)

Upscaling shallow water models for overland flow using roughness formulations

Ilhan Özgen · Katharina Teuber · Franz Simons · Dongfang Liang · Reinhard Hinkelmann

Received: date / Accepted: date

I. Özgen

Technische Universität Berlin, Chair of Water Resources Management and Modeling of Hydrosystems, Secr. TIB1–B14, Gustav–Meyer–Allee 25, 13355 Berlin, Germany

Tel.: +49-30-72428

Fax: +49-30-72430

E-mail: ilhan.oezgen@wahyd.tu-berlin.de

K. Teuber

Technische Universität Berlin, Secr. TIB1–B14, Gustav–Meyer–Allee 25, 13355 Berlin, Germany

F. Simons

Bundesanstalt für Wasserbau, Kußmaulstraße 17, 76187 Karlsruhe, Germany

D. Liang

University of Cambridge, Department of Engineering, Trumpington Street, Cambridge CB2 1 PZ, Cambridge, UK

R. Hinkelmann

Technische Universität Berlin, Secr. TIB1–B14, Gustav–Meyer–Allee 25, 13355 Berlin, Germany

Abstract This study presents a novel roughness formulation to conceptually account for microtopography and compares it to four existing roughness models from literature. The aim is to increase the grid size for computational efficiency, while capturing subgrid scale effects with the roughness formulation to prevent the loss in accuracy associated with coarse grids. All roughness approaches are implemented in the Hydroinformatics Modeling System and compared with results of a high resolution shallow water model in three test cases: rainfall-runoff on an inclined plane with sine-wave shaped microtopography, flow over an inclined plane with random microtopography and rainfall-runoff in a small natural catchment. Although the high resolution results can not be reproduced exactly by the coarse grid model, e.g. local details of flow processes can not be resolved, overall good agreement between the up-

scaled models and the high resolution model has been achieved. The proposed roughness formulation generally shows the best agreement of all compared models. It is further concluded that the accuracy increases with the number of calibration parameters available, however the calibration process becomes more difficult. Using coarser grids results in significant speedup in comparison with the high resolution simulation. In the presented test cases the speedup varies from 20 up to 2520, depending on the size and complexity of the test case and the difference in cell sizes.

Keywords upscaling · roughness formulation · shallow water equations · overland flow

1 Introduction

Recent developments in survey technology such as light detection and ranging (LIDAR) and laser scanning are able to provide high-resolution elevation data sets, yet the integration of these data into numerical models is often challenging because of finite computer resources [6, 8, 23]. The use of high-resolution elevation data is generally desirable, because it allows a better representation of spatial heterogeneity and localized flow processes. However, high-resolution simulations of practical interest, e.g. across catchment or city scales, are often unfeasible without supercomputers because they are computationally very demanding [29]. Therefore, high-resolution elevation data is usually averaged over relatively coarse grid cells [19] which results in loss of model accuracy [41].

The accuracy of coarse grid models can be improved by conceptually accounting for subgrid-scale effects by calibrating the roughness coefficient [26]. This is a valid natural approach because by definition, a roughness coefficient expresses a parameterization of subgrid topography [30]. In principal, the roughness coefficient in shallow water models represents the shear stress at the bottom of a water column but is often used to account for all unresolved processes, e.g. turbulence, depth-averaging effects, and therefore may lose its physical meaning [24]. The value of the calibrated roughness coefficient is usually heavily dependent on the calibration conditions, e.g. water depth, grid size, and can not be transferred easily to different conditions [17, 40].

Upscaling is the approximation of a system of partial differential equations by another system of partial differential equations that can be solved with fewer computing resources [7]. The upscaling process usually requires the determination of a set of coefficients, which conceptually account for properties of the original system. The main advantage of using roughness formulations instead of more sophisticated upscaling approaches for shallow water models, e.g. [9, 17, 21, 23, 38],

is their easy implementation into existing models without the need to modifiy the governing equations or numerical methods. Certainly, the more sophisticated upscaling approaches improve the model accuracy better than a simple roughness formulation.

This study presents a novel roughness formulation to account for the effects of microtopography and investigates limits and capabilities of upscaling shallow water equations based overland flow models using roughness formulations. The proposed new formulation uses the experimental studies in [20, 32, 37] as theoretical basis and is to some extent inspired by the roughness models in [18, 27]. The distribution function of the subgrid-scale bottom elevation and the water depth are used to calculate a dimensionless inundation ratio, which is then used to calculate a roughness coefficient. Further, the bottom slope is taken into account. The formulation is compared with four different roughness models: Manning's model with constant roughness coefficient; Lawrence's model [20]; Manning's model with a water-depth dependent roughness coefficient [25] and Razafison's furrow roughness model [27]. All approaches are implemented in the Hydroinformatics Modeling System (hms) [28] and evaluated in three test cases: rainfall-runoff on an inclined plane with sine-wave shaped microtopography; surface flow over an inclined plane with random microtopography; and rainfall-runoff in a small Alpine catchment.

2 Governing equations

2.1 Shallow water equations

The depth-averaged shallow water equations can be written in a conservative form as

$$\frac{\partial \mathbf{q}}{\partial t} + \frac{\partial \mathbf{f}}{\partial x} + \frac{\partial \mathbf{g}}{\partial y} = \mathbf{S}, \tag{1}$$

where t is time, x and y are the Cartesian coordinates, $\mathbf{q}$, $\mathbf{f}$ and $\mathbf{g}$ denote the vectors of conserved flow variables, fluxes in the x- and y-directions, respectively. $\mathbf{S}$ is the source vector including bed slope source $\mathbf{S}_b$ and friction source term $\mathbf{S}_f$. $\mathbf{q}$, $\mathbf{f}$ and $\mathbf{g}$ are usually expressed as

$$\mathbf{q} = \begin{bmatrix} h \\ q_x \\ q_y \end{bmatrix}, \ \mathbf{f} = \begin{bmatrix} q_x \\ uq_x + 0.5gh^2 \\ uq_y \end{bmatrix}, \ \mathbf{g} = \begin{bmatrix} q_y \\ vq_x \\ vq_y + 0.5gh^2 \end{bmatrix}. \tag{2}$$

Here, h, u, v are the water depth and depth-averaged velocity in x- and y-directions, respectively; q_x and q_y are the unit-width discharges in x- and y-directions, and $q_x = uh$, $q_y = vh$; g represents the gravity acceleration. The source vector $\mathbf{S}$ can be splitted into

$$\mathbf{S} = \mathbf{S}_b + \mathbf{S}_f + \mathbf{S}_o. \tag{3}$$

Here $\mathbf{S}_o$ accounts for additional source terms, e.g. rainfall, wind shear on the free surface, Coriolis-force. It is noted that the first entry of the vector $\mathbf{S}$ is the mass source, the second entry and third entry are momentum source terms in x- and y-direction, respectively. Writing out the vectors leads to

$$\mathbf{S} = \begin{bmatrix} 0 \\ s_{b,x} \\ s_{b,y} \end{bmatrix} + \begin{bmatrix} 0 \\ s_{f,x} \\ s_{f,y} \end{bmatrix} + \mathbf{S}_o, \tag{4}$$

$$\mathbf{S} = \begin{bmatrix} 0 \\ -gh\partial z_b/\partial x \\ -gh\partial z_b/\partial y \end{bmatrix} + \begin{bmatrix} 0 \\ -gu|\mathbf{v}|/C^2 \\ -gv|\mathbf{v}|/C^2 \end{bmatrix} + \mathbf{S}_o. \tag{5}$$

z_b stands for bottom elevation; $\mathbf{v} = \{u, v\}$ is the vector of velocity; $|\cdot|$ denotes the vector norm and C is the so-called Chézy coefficient accounting for flow resistance. As shown in, e.g. [28, 31], every friction law coefficient can be transformed into the Chézy coefficient and therefore can be incorporated in Equation 1. Viscosity of the fluid and turbulence are neglected in this study. The incorporation of these effects into the shallow water equations can be found in, e.g. [10].

2.2 Existing roughness formulations

Friction laws can be written in a generalized form as

$$\mathbf{S}_f = -Kh^{\alpha}|\mathbf{v}|^{\beta}\mathbf{v} \tag{6}$$

where α and β are positive real numbers. Well known friction laws such as, e.g. Manning's law and the Darcy-Weisbach law, can be obtained by a certain choice for α and β. When formulating a friction law, the choice of α and β is arbitrary [27], however the choice is usually related to experimental data sets.

Manning's law with constant roughness can be obtained by choosing $\alpha = -1/3$ and $\beta = 1$ in Equation 6:

$$\mathbf{S}_f = -\,n\,h^{-1/3}|\mathbf{v}|\mathbf{v} \tag{7}$$

Here, n is the Manning roughness coefficient, which relates to the Chézy coefficient as

$$C = \frac{h^{1/6}}{n}. \tag{8}$$

In Lawrence's roughness model [20], different flow regimes associated with different roughness formulations are identified for different inundation ratios. The inundation ratio Λ is calculated as

$$\Lambda = \frac{h}{k} \tag{9}$$

by using a characteristic roughness length k, which is identified as the mean grain size of the river bed. For increasing Λ, the influence of the subgrid-scale topography decreases. The frictional resistance f is calculated for $\Lambda < 1$ with a drag force approach

$$f = \frac{8\phi C_d}{\pi}\min\left(\frac{\pi}{4}, \Lambda\right), \tag{10}$$

where C_d stands for the drag coefficient for roughness elements, and ϕ is the fraction of the surface covered by roughness elements. For the drag coefficient, $C_d = 1$ is assumed [20]. The operator $\min(\cdot)$ is the minimum function, which outputs the smallest value of all input values. For $1 \leq \Lambda \leq 10$, a power law in the form of

$$f = \frac{10}{\Lambda^2} \tag{11}$$

is suggested. For $\Lambda > 10$, f is calculated with

$$f = \frac{1}{(1.64 + 0.803 \ln \Lambda)^2}. \tag{12}$$

Here, $\ln(\cdot)$ stands for the natural logarithm function. The suggested calibration parameters of this model are ϕ (cf. Equation 10) and k (cf. Equation 9) [25]. f can be transformed into the Chézy coefficient by using

$$C = \sqrt{\frac{8\,g}{f}}. \tag{13}$$

The depth-dependent variable Manning's coefficient has been developed for rainfall-runoff models in [18] and is calculated as follows:

$$n(h) = \begin{cases} n_0 \left(\frac{h}{h_0}\right)^{-\epsilon} & \text{for} \quad h < h_0, \\ n_0 & \text{for} \quad h \geq h_0 \end{cases} \tag{14}$$

In this model, n_0 is defined as the Manning's roughness occuring at flow depth h_0 beyond which n is assumed constant and ϵ is a parameter accounting for vegetation. The transformation into the Chézy coefficient is done according to Equation 8. The variable Manning's coefficient model has three calibration parameters: n_0, h_0 and ϵ.

2.3 New roughness formulation

Common roughness formulations usually express a relationship between water depth and roughness, often in the form of a power law, e.g. [18, 25, 27, 37]. In the authors opinion, a more general approach can be obtained for free surface flows by using the inundation ratio instead of the water depth and by including the unitless bottom slope into the formulation. In this study, $\alpha = 0$ and $\beta = 1$ are chosen in Equation 6, which allows to rewrite the friction source term in Equation 5 as

$$\mathbf{S}_f = -\left(\frac{g}{C_0^2} + K\right)|\mathbf{v}|\mathbf{v}. \tag{15}$$

Here, subgrid-scale topography is accounted for with the variable dimensionless roughness value K, which increases the roughness of the model in dependency of the inundation ratio, and an increased Chézy coefficient C_0.

Experimental results reported in [32] show that the bottom slope I reduces the influence of tillage significantly. This findings certainly can be extended to microtopography in general, as increasing the slope is associated with a loss of surface storage [35].

Then, Equation 15 is required to satisfy the following requirements:

1. If Λ increases, the influence of the subgrid-scale topography should decrease significantly, hence K should converge to 0.

2. If I increases, the influence of the subgrid-scale topography should decrease, hence K should decrease.
3. For large Λ, only C_0 should account for subgrid-scale effects.

C_0 is a model calibration parameter. In this study, a constant Manning formulation (Equation 8) is used to calculate C_0. Based on preliminary numerical studies by the authors [34], the following formulation for K is proposed, which satisfies these requirements:

$$K = \alpha_0 \exp\left(-\alpha_1 \ (\Lambda - 1)\right) \tag{16}$$

Here, $\exp(\cdot)$ stands for the natural exponential function. The inundation ratio is calculated by a modified expression of Equation 9 to take the effect of bottom slope into account:

$$\Lambda = \frac{h}{(1 - I) \ k} \tag{17}$$

In this study, the standard deviation of microtopography, hereinafter referred to as σ, is used as the characteristic roughness length k. σ represents a summary of topographic irregularity and is often used as a roughness indicating parameter [30,31], hence it is reasonable to use it as the characteristic roughness length. The relationship between σ and the maximum value of the distribution a_r can be approximated by $a_r = 2\,\sigma$ [4], which means that $\Lambda = 1$ does not indicate full inundation but marks the point, where the majority of the subgrid-scale topography has been inundated. For the derivation of the depth-averaged shallow water equations, I is required to be very small. In shallow water flow simulations, I is usually in the range of 0 to 0.1.

Equations 15, 16 and 17 together represent the proposed roughness formulation. To provide some physical interpretation on the calibration parameters, α_0 can be regarded as a dimensionless friction coefficient. α_1 can be interpreted as a geometric conveyance parameter. It accounts for the influence of the spatial distribution of the subgrid-scale elevations, e.g. blockade effects due to clustering mentioned in [41]. A large α_1 indicates that the conveyance of the spatial distribution is high, so K decreases faster. In the applications presented in this work, α_0 and α_1 are model calibration parameters. Thus, in total three parameters are used for model calibration; C_0, α_0, and α_1. However, as C_0 is calculated via Equation 8, the model is actually calibrated using a Manning's coefficient n.

3 Numerical implementation

The shallow water equations, shown in Equation 1, are discretized with cell-centered finite volumes. The discretized equations are solved numerically with a second order monotonic-upstream-centered scheme for conservation laws (MUSCL) as presented in [28]. For the sake of completeness, a brief overview of the implementation is given below, but it is noted that no novel contribu-

tion to the numerical methods has been made in this work.

3.1 Interface flux calculation

The fluxes at cell interfaces, given by the vectors $\mathbf{f}$ and $\mathbf{g}$ in Equation 2, are functions of the state variables h and $\mathbf{v}$. Appropriate values for the state variables are calculated by solving the Riemann problem on the interface via a Harten, Lax and van Leer approximate Riemann solver with the contact wave restored (HLLC) [36]. The Riemann states at the left and right side of the interface, namely h_L, h_R and $\mathbf{v}_L$, $\mathbf{v}_R$ where L and R stand for the left and right side of the interface, respectively, are extrapolated from the cell center with a three-point-stencil with slope limiters, shown in [14, 15]. In this study, the min-mod limiter is used to suppress spurious oscillations.

To well preserve the C-property, non-negative hydrostatic reconstruction of the bottom elevation at the interface is used [1]. The water depth and bottom elevation are modified prior to the Riemann solution [13]. Discussion of the non-negative hydrostatic reconstruction method is given in [5, 16]. Implementation details within hms are found in [28].

3.2 Slope source term treatment

The bottom slope source term $\mathbf{S}_b$ of a cell (cf. Equation 3) is transformed into fluxes through the cell faces [13]. The bottom slope flux $\mathbf{f}_{bk}$ over the edge k becomes:

$$\mathbf{f}_{bk} \cdot \mathbf{n}_k = \begin{bmatrix} 0 \\ -n_{xk} 0.5g \left(h_k + h\right)\left(z_{Bk} - z_B\right) \\ -n_{yk} 0.5g \left(h_k + h\right)\left(z_{Bk} - z_B\right) \end{bmatrix} \tag{18}$$

$\mathbf{n}_k$ is the unit normal vector of the edge k with components n_{xk}, n_{yk} in x- and y-direction respectively, defined to be positive if it points outside of the cell. The subscript k denotes that the variable is considered at the edge k. Variables without subscript k are the values at the centroid of the considered cell.

3.3 Friction source term treatment

The splitting point-implicit method derived in [22] allows a fully implicit integration of the friction source term. In this section, $\mathbf{q}$ stands for the vector of unit discharges, i.e. only the second and third entries of the vector $\mathbf{q}$ in Equation 2 are considered. The splitting point-implicit method approximates the friction source term on the next time level $n+1$ with a first order Taylor series as

$$\mathbf{S}_f^{n+1} = \mathbf{S}_f^n + \left(\frac{\partial \mathbf{S}_f}{\partial \mathbf{q}}\right)^n \Delta\mathbf{q} + O\left(\Delta\mathbf{q}^2\right), \tag{19}$$

where $\Delta\mathbf{q} = \mathbf{q}^{n+1} - \mathbf{q}^n$. The point-implicit formulation of the equations of momentum in the shallow water

equations (Equations 1 and 2) is written as

$$\frac{\mathbf{q}^{n+1}-\mathbf{q}^{n}}{\Delta t} = -\frac{1}{A}\sum_{k}\mathbf{f}_k^n\mathbf{n}_k\Delta k + \mathbf{S}_f^{n+1}. \tag{20}$$

Substituting Equation 19 into Equation 20 gives

$$\frac{\Delta\mathbf{q}}{\Delta t} = -\frac{1}{A}\sum_{k}\mathbf{f}_k^n\mathbf{n}_k\Delta k + \mathbf{S}_f^{n} + \left(\frac{\partial\mathbf{S}_f}{\partial\mathbf{q}}\right)^n\Delta\mathbf{q}. \tag{21}$$

Δk is the length of edge k and A is the area of the cell. Rearranging Equation 21 leads to

$$\left(\mathbf{I}-\left(\frac{\partial\mathbf{S}_f}{\partial\mathbf{q}}\right)^n\right)\frac{\Delta\mathbf{q}}{\Delta t} = -\frac{1}{A}\sum_{k}\mathbf{f}_k^n\mathbf{n}_k\Delta k + \mathbf{S}_f^{n}, \tag{22}$$

where $\mathbf{I}$ is the identity matrix. $\partial\mathbf{S}_f/\partial\mathbf{q}$ is usually referred to as the Jacobian matrix of the friction source term. Further, if the matrix $\mathbf{PI}$ is defined to be

$$\mathbf{PI} = \left(\mathbf{I}-\left(\frac{\partial\mathbf{S}_f}{\partial\mathbf{q}}\right)^n\right), \tag{23}$$

then Equation 21 can be rewritten as

$$\mathbf{q}^{n+1} = \mathbf{q}^{n} + (\mathbf{PI})^{-1}\left(-\frac{\Delta t}{A}\sum_{k}\mathbf{f}_k^n\mathbf{n}_k\Delta k + \Delta t\mathbf{S}_f^n\right), \tag{24}$$

where $(\cdot)^{-1}$ is the inversion of a matrix.

In order to avoid numerical instabilites caused by too high friction source terms, the entries $s_{f,x}$ and $s_{f,y}$ of the vector $\mathbf{S}_f$ (cf. Equation 5) are limited as shown in [22]:

$$s_{f,i}\begin{cases}\geq -q_i^n\Delta t & \text{if } q_i^n \geq 0\\ \leq -q_i^n\Delta t & \text{if } q_i^n < 0\end{cases} \tag{25}$$

Here, the subscript i stands for either x or y, denoting the direction in cartesian coordinates. With this limitation, friction no longer changes the direction of the flow [13].

4 Computational examples

All simulations were carried out with the Hydroinformatics Modeling System (hms), an in-house scientific prototyping framework [28]. The proposed roughness approach is compared with results of different roughness models and a high-resolution model with explicitly discretized microtopography, called HR model in the following. The parameters of all models are optimized with the SciPy library [39] by minimizing the RMSD of the model results in regard to the HR model, using either Brent's method [2] for one free parameter or the Limited-memory Broyden, Fletcher, Goldfarb and Shanno algorithm (L-BFGS-B) [3, 42] for more parameters.

Model results are evaluated using the root mean square deviation (RMSD) which is calculated as:

$$\text{RMSD} = \sqrt{\frac{\sum_{t=1}^{n}\left(\hat{q}_t - q_t\right)^2}{n}} \tag{26}$$

Here, $\hat{q}_t$ is the roughness model result value, q_t stands for the value of the reference solution of a HR model; t is a sample index and n is the number of samples. The normalized root mean square deviation NRMSD is

calculated as

$$\mathrm{NRMSD} = \frac{\mathrm{RMSD}}{q_{\max} - q_{\min}}, \tag{27}$$

where $q_{\max}$ and $q_{\min}$ are the maximum and minimum values of the reference solution calculated by the HR model, respectively.

4.1 Rainfall-runoff over an inclined plane with sine-wave shaped microtopography

One-dimensional rainfall-runoff over an inclined plane with sine-wave shaped microtopography is simulated. Although synthetic, this test case is suitable to study the capability of roughness models because in the limit, any theory for complex microtopography has to converge to the solution of this idealized set up [35]. The domain is 4 m long and its topography is described by

$$z_b = -0.05\,x + 0.01\,\mathrm{sim}\left(20\pi\,x + \frac{\pi}{2}\right) \tag{28}$$

for a high-resolution model with explicitly discretized microtopography (HR) on a 0.01 m grid. The standard deviation of the microtopography is $\sigma = 0.01$ m. Results for the proposed roughness model (RM), Lawrence's model (LAW), constant Manning's coefficient model (CM) and variable Manning's coefficient model (VM) using a grid size of 0.1 m are calculated.

The topography for these models is described by

$$z_b = -0.05\,x. \tag{29}$$

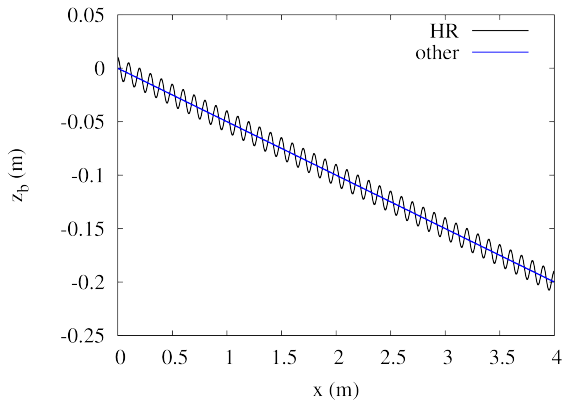

Fig. 1 Rainfall-runoff over an inclined plane with sine-wave shaped microtopography: Computational domain of different models: HR (black), all other models (blue).

Additionally, the model results presented in [27] (RA) for this test case on a 0.1 m grid are given for comparison. The RA model also uses the topography calculated by Equation 29. The side-view of the domain with microtopography (HR) and without (other) is plotted in Figure 1. At $x = 4$ m, an open boundary condition which forces the gradient of water depth to be equal to the gradient of bottom elevation is imposed. All other boundaries are closed walls. The roughness is expressed via a Manning's coefficient of $n = 0.04\,\mathrm{sm}^{-1/3}$. Rainfall is imposed with a constant intensity of $i = 8 \cdot 10^{-4}$ m/s for a duration of 22.5 s. The RA model is developed for furrows and calculates the friction coefficient K_{R} as follows:

$$K_{\mathrm{R}} = K_{0,\mathrm{R}} \exp\left(\frac{-h + \langle h_F \rangle}{C \cdot \langle h_F \rangle}\right) \tag{30}$$

Here, $K_{0,\mathrm{R}}$ and C are unitless model parameters; and $\langle h_F \rangle$ is the average height of water trapped in furrows which may be calculated with

$$\langle h_F \rangle = \frac{V}{L_F \cdot L}, \tag{31}$$

whereby V is the volume of trapped water in a furrow, L_F is its wavelength and L is the length of the domain. Razafison suggests to approximate $\langle h_F \rangle$ numerically (personal communication, August 4, 2014). The optimal parameters of the RA model for this test case were taken from the literature [27]. The unit discharges at the outlet of the domain divided by the total unit discharge of the rain $q_{\mathrm{rain}} = 3.2 \cdot 10^{-3}\,\mathrm{m}^2/\mathrm{s}$ are plotted in Figure 2. Optimiziation was carried out regarding the discharge at the outlet of the domain. The optimized parameters for each model together with the resulting RMSDs are given in Table 1. The CM model poorly reproduces the HR model result by overshooting it in the early stage of the simulation and undershooting it in the later stage. The VM model with three free parameters shows very good agreement. The RM model shows the best agreement. At the beginning, the HR model results are slightly overshot however in the later stages the curves show very good agreement. The LAW model with two calibration parameters shows good agreement with the HR model. The discharge in the early stages of the simulation is overshot by the LAW model, however the later stages are captured well. The discharge calculated by the RA model rises later than all other models and keeps undershooting the HR model results. A discontinuity occurs at about $t = 20\,\mathrm{s}$, which marks the time for $\langle h_F \rangle < h$. At the end of the simulation, the RA model catches up with the HR model.

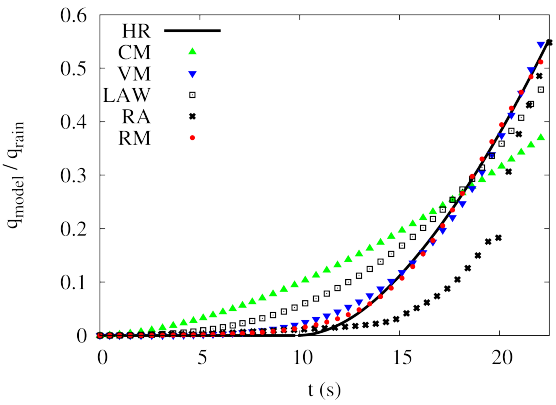

Fig. 2 Rainfall-runoff over an inclined plane with sine-wave shaped microtopography: Unit discharges compared at the outlet.

Table 1 Rainfall-runoff over an inclined plane with sine-wave shaped microtopography: Calibrated parameter values and corresponding RMSD for each model.

Model	Calibrated parameter(s)	RMS
CM	$n = 0.22\,\mathrm{sm}^{-1/3}$	0.081
VM	$n_0 = 0.018\mathrm{sm}^{-1/3}$;$h_0 = 0.04\mathrm{m}$;$\epsilon = 2.4$	0.014
LAW	$\phi = 5.6\,\%$; $k = 0.06\,\mathrm{m}$	0.040
RA	$C = 0.4$; $K_{0,\mathrm{R}} = 0.02$	0.058
RM	$n = 0.15\,\mathrm{sm}^{-1/3}$;$\alpha_0 = 28.57$;$\alpha_1 = 7.26$	0.007

All models can be calibrated to match the HR results to some extent. However, it could be argued that the VM model parameter h_0 and the LAW model pa-

rameter k are geometric parameters and should not be used for calibration. From their conceptual point of view, h_0 and k should either be set to the standard deviation of microtopography, i.e. 0.01 m, or the amplitude of the microtopography, i.e. 0.02 m. It was found out that using these values for h_0 and k significantly reduces these models accuracy. Especially the LAW model can not be calibrated to satisfactory accuracy using only ϕ, because ϕ represents a fraction and therefore is bounded between 0 and 1 and is not very sensitive. The simulation of the coarse models runs on a mesh with 40 cells in average 50 times faster than the HR model simulation, which runs on a mesh with 400 cells.

4.2 Flow over an inclined plane with random microtopography

The following example simulates a run-dry process of an inclined surface with random microtopography. The domain is initally ponded with water which is then discharged during the simulation at the outlet of the domain. No rainfall is imposed. The study area is a $4\,\mathrm{m} \times 1\,\mathrm{m}$ inclined plane with a Manning coefficient of $n = 0.02\ \mathrm{sm}^{-1/3}$ (cf. Figure 3 (top)). Random microtopography is generated as square blocks with a horizontal length of 0.05 m and a vertical elevation according to a Gaußian distribution with a standard deviation of $\sigma = 0.02$ m (cf. Figure 3 (bottom)). The maximum value of the microtopography is about 0.07 m and the minimum value about -0.08 m. Several simulations with different slope and initial water depth are carried out. The slope I is varied in steps of 0.01 from -0.01 to -0.14 for different simulation runs. For each different slope, different simulation runs with varying initial water depth h_0 from 0.005 m to 0.08 m in 0.005 m-steps are carried out. For example, for $I = -0.01$, simulation runs with $h_0 = 0.005\,\mathrm{m}$, $h_0 = 0.01\,\mathrm{m}$, $h_0 = 0.015\,\mathrm{m}$ until $h_0 = 0.08\,\mathrm{m}$ are carried out, and after that the slope is set to $I = -0.02$ and again simulation runs with varying h_0 are carried out. The boundary condition at the outlet is an open boundary which sets the gradient of water depth equal to the gradient of bottom elevation, all other boundaries are closed walls. The simulation runs for $t = 60$ s. Four different roughness models are compared for every possible combination of I and h_0 with results of a high-resolution model explicitly discretizing the microtopography (HR): a model using a calibrated constant Manning's coefficient (CM); a model using a variable Manning's coefficient (VM), Lawrence's model (LAW); and the proposed roughness approach (RM). The HR model uses quadratic grid cells with an edge length of 0.01 m, all other models use grids with coarser cells.

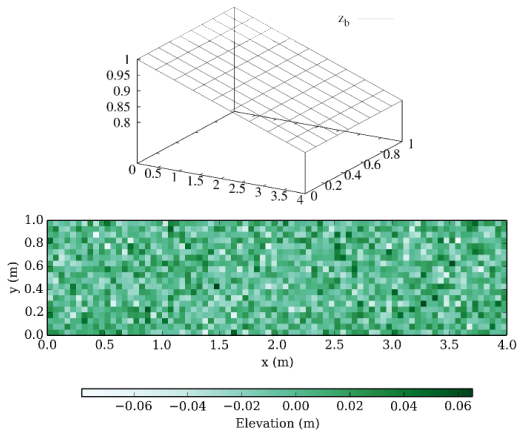

Fig. 3 Flow over an inclined plane with random microtopography: Global topography for $I = 0.05$ (top); microtopography (bottom).

All models were calibrated on a $0.05\,\mathrm{m} \times 0.05\,\mathrm{m}$-grid with regard to the unit discharge calculated by the HR model at the outlet of the domain for a slope of $I = -0.02$ and an initial water depth of $h_0 = 0.04\,\mathrm{m}$, i.e. an initial inundation ratio of $\Lambda_0 = h_0/\sigma = 2$. First, a simulation on the $0.05\,\mathrm{m} \times 0.05\,\mathrm{m}$ grid using the same roughness coefficient as the HR model ($n = 0.02\,\mathrm{sm}^{-1/3}$) is carried out (UCM), to show the effects of increasing the grid size without using an upscaling approach. Results for the unit discharge at the outlet for the UCM model run are plotted in Figure 4 (top). The peak of the discharge curve of the UCM model is about 20 times higher than the HR model. After the peak is reached, the UCM model discharge decreases too quickly which indicates that the roughness is overall underestimated. A NRMSD of 1.0 is calculated.

The calibrated parameters of all models with the corresponding NRMSDs are given in Table 2. The unit discharges at the outlet are plotted in Figure 4 (bottom). While the LAW model is showing the worst agreement with the HR model, the VM model agrees the best, followed by the RM model. Although the first peak of the HR model can not be captured by any of the models, overall the VM and RM models capture the HR model results very well. The CM model undershoots the HR solution significantly at the beginning of the simulation and starts to overshoot it after about $t = 12\,\mathrm{s}$. The overall agreement is not satisfactory. Additional calibrations which were carried out with different initial conditions suggest that all models except the LAW model should be calibrated for $\Lambda_0 \geq 2$, because for $\Lambda_0 < 2$ the calibration may fail to deliver good results. One reason for this may be, that for $\Lambda_0 < 2$ the blockade effects of the microtopgraphy outweigh its roughness effects, i.e. the flow depends on the spatial configuration and geometric properties of single microtopography elements. Then, spatial heterogeneity significantly influences the flow and therefore the roughness effects can not be averaged over the domain. For $h_0 = 0.04\,\mathrm{m}$, the LAW model uses Equation 11 to calculate the roughness and therefore has no calibration parameters. The calibrated values in Table 2 effect only the stage of the simulation when the inundation ratio

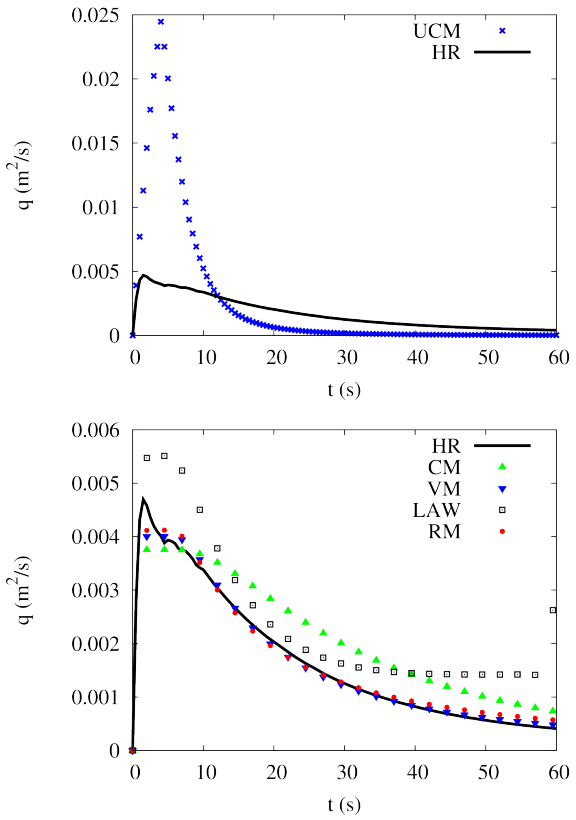

Fig. 4 Flow over an inclined plane with random microtopography, 0.05 m grid size: Unit discharges of the UCM and HR models (top) and all models except UCM (bottom) compared at the outlet for $h_0 = 0.04$ m and $I = 0.02$.

becomes smaller than 1. Calibrating the LAW model for smaller Λ_0 might deliver better results, however the calibration difficulties regarding the LAW model mentioned in the test case before still remain.

To study the transferability of the calibrated parameters to different hydraulic conditions, the calibrated parameters in Table 2 are used to simulate the unit discharge for every I-Λ_0 combination. The grid cell size used by the models is 0.05 m. Results are compared with HR model results. Figure 5 shows the NRMSD

Table 2 Flow over an inclined plane with random microtopography, 0.05 m grid size: Calibrated parameter values and corresponding NRMSD for $h_0 = 0.04$ m and $I = 0.02$ for each model.

Model	Calibrated parameter(s)	NRMS
CM	$n = 0.18\,\mathrm{sm}^{-1/3}$	0.120
VM	$n_0 = 0.14\mathrm{sm}^{-1/3}$;$h_0 = 0.045\mathrm{m}$;$\epsilon = 1.4$	0.026
LAW	$\phi = 50\,\%$; $k = 0.023\,\mathrm{m}$	0.173
RM	$n = 0.112\mathrm{sm}^{-1/3}$;$\alpha_0 = 5.52$;$\alpha_1 = 2.61$	0.030

of all models in dependency of I and Λ_0, where each cell is the result of a simulation run of a certain I-Λ_0 combination. The main focus of Figure 5 is the change of the NRMSD in dependency of I and Λ_0 within one model. Because of this reason and the significant differences in the NRMSDs of different models, the range of the legends are not set equal. The I-Λ_0 combination used for the calibration is denoted with a black rectangle. High NRMSD in the CM model results occur for small Λ_0 combined with small I. As Λ_0 or I increase, the NRMSD decreases as the influence of the microtopography decreases. The minimum NRMSD occurs for the calibration conditions, i.e. $\Lambda_0 = 2$ and $I = -0.02$. Except for the region around $\Lambda_0 = 0.75$ and $I = -0.01$, which is the location of the maximum NRMSD, the transfer of the calibrated parameters to different I and Λ_0 does not significantly alter the NRMSD. It stays almost constant around the mean value of 0.133. The

NRMSD distributions of the VM model and the RM model are qualitatively very similar. High NRMSD occurs for small Λ_0 combined with large I. For the VM model, the minimum NRMSD occurs for the calibration conditions, but for the RM model smaller NRMSD is calculated for other simulation runs. For both models, transfering the calibrated parameters to hydraulic conditions with $\Lambda_0 > 1.5$ leads to increased NRMSDs, but transfering the parameters to conditions with higher Λ_0 has not a significant influence on the NRMSD. The LAW model has the highest NRMSD of all considered models. The NRMSD increases significantly for $\Lambda_0 < 1$, for $\Lambda_0 > 1$ the NRMSD is about 0.15 and remains constant. With increasing Λ_0, the NRMSD decreases. The maximum NRMSD, the minimum NRMSD and the mean NRMSD of all simulations for each model are given in Table 3. Here it is seen that the RM model calculates a smaller minimum, maximum, and mean NRMSD than the VM model, but the VM model can be locally calibrated to show better agreement (cf. Figure 4 (bottom)).

Grid size is increased from 0.05 m to 0.1 m and to 0.2 m to study the transferability of the calibrated parameters to different meshes. It is desirable, that the RMSD decreases with decreasing cell size (which is also called grid convergence) because this allows to efficiently calibrate the model on coarser cells and then transfer the calibrated parameters to a model with the desired spatial resolution [12]. If this can not be achieved, it is desirable that at least the RMSD stays the same for different cell sizes. Table 4 shows the NRMSD in dependency of grid cell length averaged over all I-Λ_0-combinations. The calibration of all models is stable across the investigated scales. The change in the NRMSD is negligable. Oddly, coarsening the grid size to 0.2 m improves the NRMSD. The reason for this negligibly small improvement may be due to numerical round-off somehow benefiting the accuracy of the solution, yet this has not been further investigated. The inclined plane as a study area is not very sensitive to grid size, because the geometry is captured perfectly accurate by the second order discretization in combination with the non-negative hydrostatic reconstruction (cf. [28]). The plane has no other spatial heterogeneities than the subgrid-scale microtopography, which is accounted for

Table 3 Flow over an inclined plane with random microtopography, 0.05 m grid size: Minimum (min), maximum (max) and mean NRMSD values of all I-Λ_0-combinations for different models.

Model	min	max	mean
CM	0.095	0.468	0.133
VM	0.026	0.347	0.105
LAW	0.093	1.688	0.335
RM	0.022	0.304	0.091

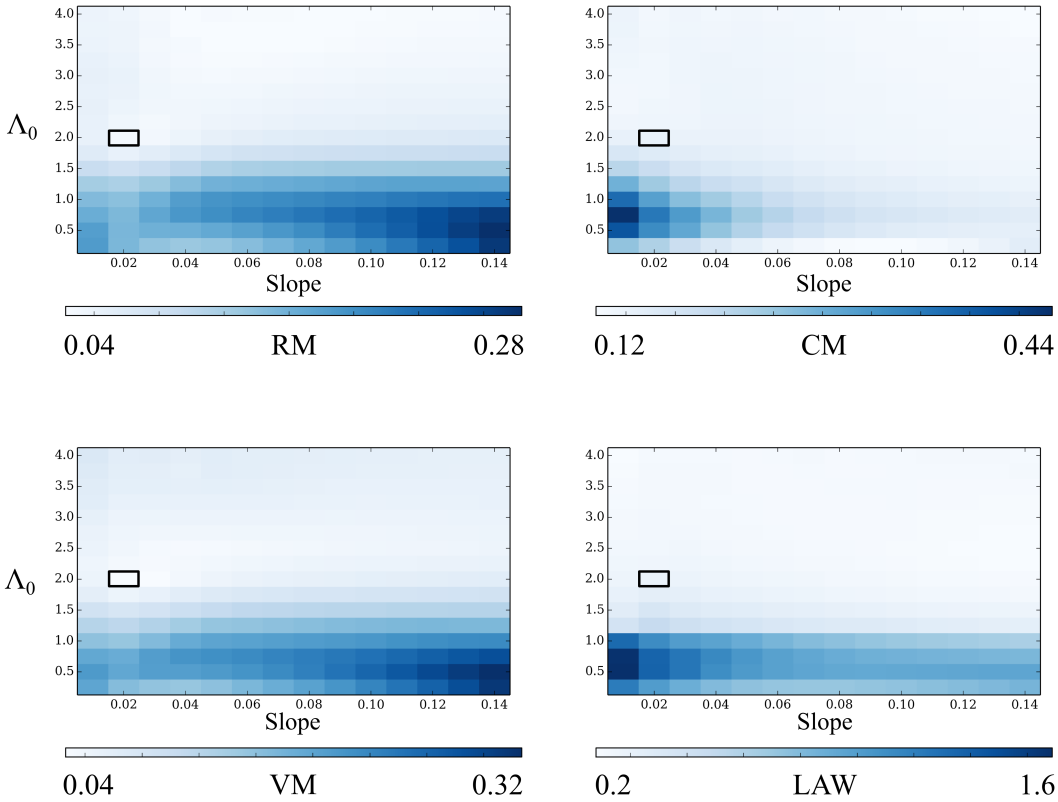

Fig. 5 Flow over an inclined plane with random microtopography, 0.05 m grid size: Normalized root mean square deviation in relation to initial inundation ratio Λ_0 and slope I.

by the roughness formulation, i.e. the model domain is a smooth inclined plane. Therefore, increasing grid size is not associated with further loss of geometric information and only reduces accuracy because of numerical diffusion. The HR model simulation runs on a mesh with 40000 cells. The simulation on the mesh with 0.05 m cell size (1600 cells) runs about 20 times faster than the HR model simulation, the simulation on the mesh with 0.1 m cell size (400 cells) runs about 40 times faster than the HR model and finally the simulation on the mesh with 0.2 m cell size (100 cells) runs about 70 times faster than the HR model simulation.

Table 4 Flow over an inclined plane with random microtopography: Mean NRMSD in dependency of grid cell length averaged over all I-Λ_0-combinations.

Model	0.05 m	0.1 m	0.2 m
CM	0.133	0.133	0.133
VM	0.105	0.105	0.105
LAW	0.336	0.336	0.335
RM	0.092	0.092	0.091

4.3 Rainfall-runoff in a small alpine catchment

4.3.1 Study area and preliminary studies

Hortonian overland flow in a natural catchment, the Heumöser slope, Vorarlberg Alps, Austria, is simulated. The study area is a 100 000 m^2 large subcatchment of the Heumöser slope. Bottom elevation of the area is provided in 1 m × 1 m resolution by a digital elevation model of the Austrian department Torrent and Avalanche Control, representing the high-resolution model. Figure 6 (top) shows the topography of the domain and the location of the outlet, where discharge was measured. Rainfall is imposed according to a time series measured in July 2008 with a resolution of 10 min (Figure 6 (middle)). The simulation runs for $t = 120$ h, i.e. 5 days.

Extensive numerical simulations of surface and subsurface runoff for this domain were carried out in [28,33] within Research Unit 'Coupling of flow and deformation processes for modelling the movement of natural slopes' funded by the German Research Foundation [11]. During these simulations, the model was calibrated with a runoff coefficient $\Psi = 0.3$ in combination with a linear reservoir model to account for the slower discharge component in the subsurface, which was identified as a crucial contributor to the discharge at the outlet of the domain. The linear reservoir is described by the following equations:

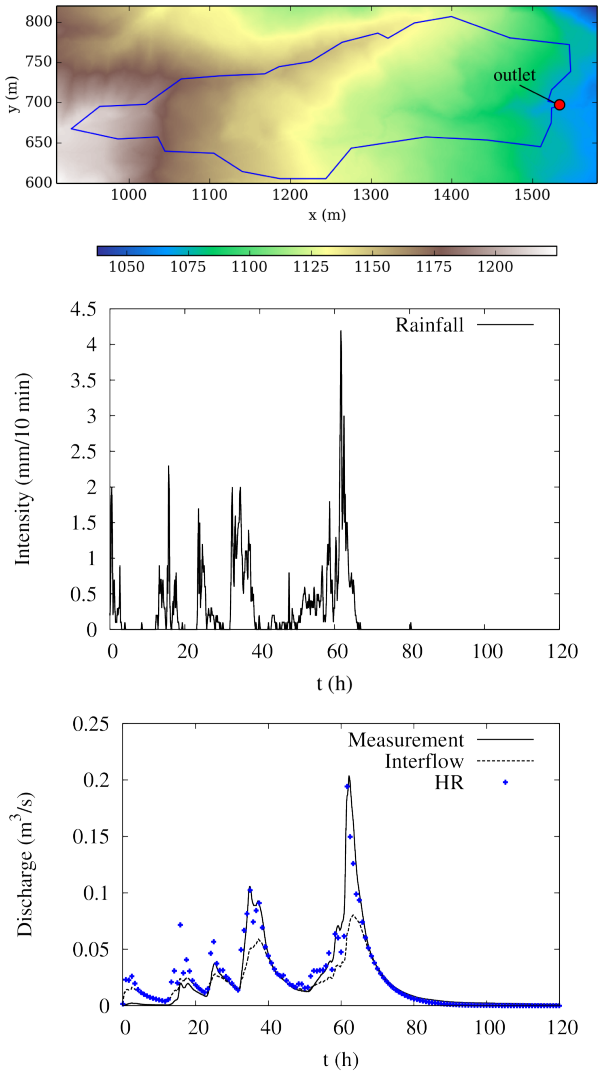

Fig. 6 Rainfall-runoff in a small alpine catchment: Bottom elevation, watershed (blue) and location of the outlet (top); intensity of the rainfall event plotted over time (middle); HR model results with parameters from [28] (bottom)

$$\frac{\mathrm{d}S(t)}{\mathrm{d}t} = I(t) - Q(t) \tag{32}$$

$$S(t) = KQ(t) \tag{33}$$

Here, $S(t)$ stands for the storage at time t; $I(t)$ for the inflow; and $Q(t)$ for the outflow of the reservoir.

K is the constant of proportionality which can be obtained by calibration. A calibration in [28] resulted in a constant of proportionality $K = 6$ h and a Manning coefficient of $n = 0.067$ sm$^{-1/3}$. Because the same numerical model (hms) as in [28] is used in this study, the same values for Ψ and K are used in all models. For reference, the results of a high-resolution simulation with these parameters on a 1 m × 1 m grid (HR) is plotted in Figure 6 (bottom).

4.3.2 Upscaling with roughness formulations

The proposed roughness formulation (RM) and three other roughness approaches are compared in this test case: calibrated constant Manning's coefficient (CM), variable Manning's coefficient (VM) and Lawrence's model (LAW). Model discharges at the outlet are superposed with the interflow computed by the linear reservoir (cf. Equations 32 and 33) and are compared with measurement data. Models are calibrated for a quadratic grid with a cell size of 10 m. In additional simulation runs, the grid size is refined to 5 m and then coarsened to 20 m, while the same model parameters were kept constant. The bottom elevation inside a cell is set to the arithmetic average of all DEM points located inside the cell. The discretization is shown in Figure 7 and will be further discussed later. In addition, the RM model requires the standard deviation of the microtopography.

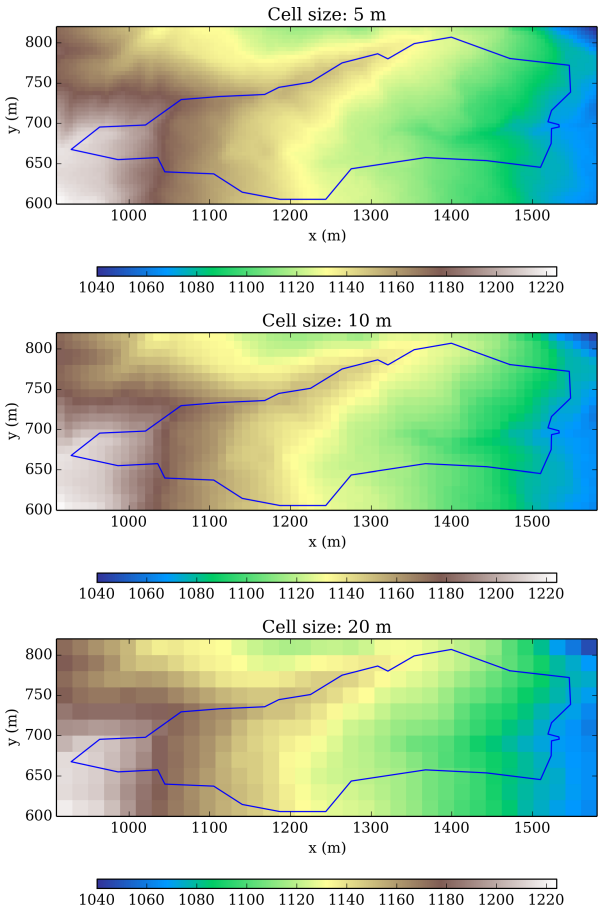

Fig. 7 Rainfall-runoff in a small alpine catchment: Bottom elevation discretization in dependency of mesh resolution

Therefore, the microtopography is isolated by calculating the deviations of each DEM point in a cell from the bottom elevation of the cell. The standard deviation of the microtopography is then calculated as $\sigma = 0.19$ m for a grid cell size of 5 m and $\sigma = 0.21$ m for a grid cell size of 10 m and 20 m.

The discretized bottom elevation for the investigated cases is given in Figure 7. As expected, the discretization with a cell size of 5 m (Figure 7 (top)) has the most information about local details in the topography.

Table 5 Rainfall-runoff in a small alpine catchment, 10 m grid size: Calibrated parameter values and corresponding RMSD for each model

Model	Calibrated parameter(s)	RMS
HR	$n = 0.067\,\mathrm{sm}^{-1/3}$	0.011
CM	$n = 0.115\,\mathrm{sm}^{-1/3}$	0.010
VM	$n_0 = 0.01\mathrm{sm}^{-1/3}$;$h_0 = 0.058\mathrm{m}$;$\epsilon = 0.11$	0.012
LAW	$\phi = 10\,\%$; $k = 0.21\,\mathrm{m}$	0.012
RM	$n = 0.035\mathrm{sm}^{-1/3}$;$\alpha_0 = 0.3$;$\alpha_1 = 0.87$	0.010

It also can be seen that the discretization with a cell size of 10 m (Figure 7 (middle)) still represents an acceptable amount of local heterogeneities and even the discretization with a cell size of 20 m (Figure 7 (bottom)) is able to capture the main topologic characteristics of the catchment. However, in the latter case the watershed boundaries start to blur and the location of the measurement weir is captured in a single cell. Small scale preferential flow paths in the domain as observed in [28] can not be represented by the coarse resolution. Additionally, numerical diffusion increases due to the mesh resolution effects [41]. All these effects have to be captured to some extent by the roughness formulations.

Table 5 shows the calibrated model parameters and the corresponding RMSD with regard to measurement data for each model. All models have almost the same RMSD, however the RM model ans the CM model give the lowest RMSD. The HR model results in a similar RMSD as the coarse models. The reason is that due to computational restraints, the HR model was calibrated manually with fewer trials than an optimization algorithm would require [28]. The usage of numerical optimization algorithms to calibrate the HR model would demand unfeasibly high computational effort. The resulting hydrographs are plotted in Figure 8 (blue triangles). In the early stages of the rainfall event, the interflow is overestimated by the linear reservoir (cf. Figure 6 (bottom)) and thus, the model results overshoot the measured data significantly. Reason for this deviation might be previous hydrological events in the catchment, which can not be taken into account. This can be seen in Figure 6 (bottom), where at the beginning of the simulation the interflow overshoots the measured time series. Most likely, in the real event the rainfall infiltrated into the groundwater instead of becoming part of the interflow. Better results might be obtained by using a more sophisticated approach than a constant runoff coefficient to estimate the effective rainfall. At around $t = 20\,\mathrm{h}$ the deviation between model and measurement begins to decrease. After $t = 30\,\mathrm{h}$, the hydrograph is captured quite accurately by the models. The CM model shows good agreement for the calibrated cell size. Both peaks are captured well. The VM model captures both occuring peaks (at about $t = 35\,\mathrm{h}$ and $t = 65\,\mathrm{h}$) the best. The LAW model and the RM model

Table 6 Rainfall-runoff in a small alpine catchment: RMSD for each model in dependency of cell size

Model	5 m	10 m	20 m
CM	0.015	0.010	0.013
VM	0.012	0.012	0.012
LAW	0.013	0.012	0.014
RM	0.016	0.010	0.013

tend to undershoot both peaks. However, the RM model captures the tails of both curves more accurately.

In order to investigate the transferability of calibrated parameters to different resolutions, cell size is varied to 5 m and 20 m. Table 6 shows the RMSD for each model in dependency of cell size. In Figure 8, the hydrographs for a cell edge length of 5 m (red circle) and a cell edge length of 20 m (black square) are plotted. For the CM model, varying the cell size decreases both peaks and decreases the arrival time of the first wave. In Table 6 it can be seen that the RMSD increases with varying cell size. For the VM model, increasing or decreasing the cell size lowers both peaks (Figure 8). For the LAW model, mesh refinement leads to an overall increase in discharge and increasing the cell size leads to an overall decrease in the discharge. Varying the cell size for the RM model leads to a significant decrease in both peaks. The arrival time of both waves is captured accurately in all cases. In Table 6 it can be seen that the VM model shows good transferability, while

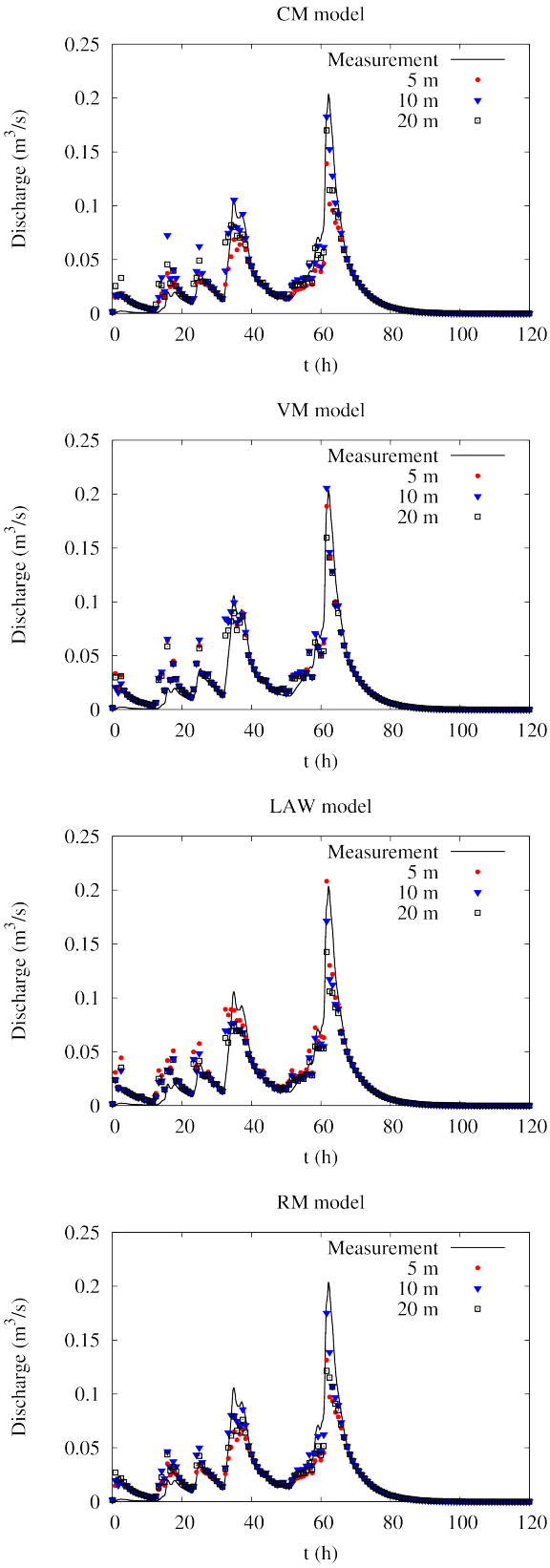

Fig. 8 Rainfall-runoff in a small alpine catchment: Discharges of different models

the calibration of the CM, LAW and RM model results show higher RMSDs if the cell size is changed.

A manual calibration of the RM model was carried out to further investigate this models parameters transferability. It was found out that the transferability of the parameters of the RM model can be increased if accuracy is sacrificed. For the parameters $n = 0.07\,\mathrm{sm}^{-1/3}$, $\alpha_0 = 0.51$ and $\alpha_1 = 0.54$, which result in a RMSD = 0.012, the RM model showed good transferability of its parameters across the investigated cell sizes.

Finally, the significant speedup gained by increasing the cell size should be emphasized. The HR model run with 147400 cells was completed in 3.5 days. Increasing cell size to 5 m reduced the cell count to 5896 cells and a computational time of 1.5 h (56 times faster). The simulations on grids with a cell size of 10 m result in 1474 cells and are on average completed in 15 min (336 times faster). Increasing the cell size to 20 m further reduces the cell number to 374 and leads to a computational time of 2 min, i.e. about 2520 times faster than the HR model. Of course the computational time depends on the hardware and the numerical code, however the speedup certainly can be transferred with little variance to different hardware and codes.

5 Conclusions

A novel conceptual roughness formulation for shallow water simulations on coarse grids was developed. The formulation is dependent on the inundation ratio, which is calculated using the standard deviation of the microtopography with regard to its mean value. A physical interpretation of the free parameters was given: the parameter C_0 is an increased Chézy coefficient, α_0 is an additional dimensionless roughness coefficient accounting for the microtopography and α_1 is a geometric conveyance parameter. The presented roughness formulation was then compared to several existing roughness formulations from literature. It was demonstrated in three computational examples, that high-resolution results can be approximated with satisfactory accuracy by calibrating the roughness formulation parameters. The exact values of the calibration parameters may vary in dependency of the numerical methods used to solve the equations, hence the optimized parameters reported in this study should be taken with a grain of salt.

The first example studied one-dimensional rainfall-runoff over a sine-wave shaped microtopography. The presented roughness approach returned the lowest root mean square deviation from the high-resolution model results. In the second example, calibrated parameters were transferred to different hydraulic conditions with

some success. Varying the slope or the initial inundation increased the error for all models. The presented roughness formulation, together with the variable Manning's coefficient, resulted in the lowest root mean square deviations. It was shown that the proposed roughness formulation can be calibrated more accurately than the variable Manning's coefficient formulation, however the latter showed a better calibration stability. In the last example, the proposed roughness approach was tested for a real case application. Here, again the presented roughness formulation and the variable Manning's coefficient approach were shown to be good trade-offs between accuracy and computational efficiency. It was shown that it is possible to upscale shallow water models using suitable roughness formulations. Due to mesh resolution effects [12, 41], the coarse grid models are not able to reproduce the high-resolution solutions exactly. In general, it can be concluded that accuracy increases with the number of free calibration parameters. However, as the number of parameters increases, the calibration process becomes more difficult. The computational benefit of using coarser cells is significant. The speedup varied from 20 to 2520 in dependency of the size and complexity of the test case and the difference in cell sizes.

Acknowledgements The authors thank the Alexander von Humboldt-Foundation for the Humboldt Research Fellowship granted to Dr. Dongfang Liang. Parts of the numerical simulations were computed on the supercomputers of Norddeutscher Verbund für Hoch- und Höchstleistungsrechnen in Berlin. The authors are grateful to Ulrich Razafison from Université de Franche-Comté, France for the correspondence on his shallow water model.

References

1. Audusse, E., Bouchut, F., Bristeau, M.O., Klein, R., Perthame, B.: A Fast and Stable Well-Balanced Scheme with Hydrostatic Reconstruction for Shallow Water Flows. SIAM Journal on Scientific Computing **25**(6), 2050–2065 (2004). DOI 10.1137/S1064827503431090
2. Brent, R.P.: Algorithms for Minimization without Derivatives. Prentice-Hall, Englewood Cliffs, New Jersey (1973)
3. Byrd, R.H., Lu, P., Nocedal, J.: A Limited Memory Algorithm for Bound Constrained Optimization. SIAM Journal on Scientific and Statistical Computing **16**(5), 1190–1208 (1995)
4. Defina, A.: Two-dimensional shallow flow equations for partially dry areas. Water Resources Research **36**(11), 3251–3264 (2000). DOI 10.1029/2000WR900167
5. Delestre, O., Cordier, S., Darboux, F., James, F.: A limitation of the hydrostatic reconstruction technique for Shallow Water equations. Comptes Rendus Mathematique **350**(13-14), 677–681 (2012). DOI 10.1016/j.crma.2012.08.004
6. Dottori, F., Di Baldassarre, G., Todini, E.: Detailed data is welcome, but with a pinch of salt: Accuracy, precision, and uncertainty in flood inundation modeling. Wa-

ter Resources Research **49**(9), 6079–6085 (2013). DOI 10.1002/wrcr.20406

7. Farmer, C.L.: Upscaling: a review. International Journal for Numerical Methods in Fluids **40**(1-2), 63–78 (2002). DOI 10.1002/fld.267. URL http://doi.wiley.com/10.1002/fld.267
8. Gourbesville, P.: Data and hydroinformatics: new possibilities and challenges. Journal of Hydroinformatics **11**(34), 330–343 (2009). DOI 10.2166/hydro.2009.143
9. Guinot, V., Soares-Frazão, S.: Flux and source term discretization in two-dimensional shallow water models with porosity on unstructured grids. International Journal for Numerical Methods in Fluids **50**(3), 309–345 (2006). DOI 10.1002/fld.1059
10. Hinkelmann, R.: Efficient Numerical Methods and Information-Processing Techniques in Environment Water. Springer Verlag, Berlin (2005)
11. Hinkelmann, R., Zehe, E., Ehlers, W., Joswig, M.: Special Section on Landslides: Setting the Scene and Outline of Contributing Studies. Vadose Zone Journal **10**(2), 473 (2011). DOI 10.2136/vzj2011.0032
12. Horritt, M.S., Bates, P.D.: Effects of spatial resolution on a raster based model of flood flow. Journal of Hydrology **253**, 239–249 (2001)
13. Hou, J., Liang, Q., Simons, F., Hinkelmann, R.: A 2D well-balanced shallow flow model for unstructured grids with novel slope source term treatment. Advances in Water Resources **52**, 107–131 (2013). DOI 10.1016/j.advwatres.2012.08.003
14. Hou, J., Simons, F., Hinkelmann, R.: Improved total variation diminishing schemes for advection simulation on arbitrary grids. International Journal for Numerical Methods in Fluids **70**(3), 359–382 (2012). DOI 10.1002/fld.2700
15. Hou, J., Simons, F., Hinkelmann, R.: A new TVD method for advection simulation on 2D unstructured grids. International Journal for Numerical Methods in Fluids **71**(10), 1260–1281 (2013). DOI 10.1002/fld.3709
16. Hou, J., Simons, F., Liang, Q., Hinkelmann, R.: An improved hydrostatic reconstruction method for shallow water model. Journal of Hydraulic Research (June), 1–8 (2014). DOI 10.1080/00221686.2013.858648
17. Hughes, J., Decker, J., Langevin, C.: Use of upscaled elevation and surface roughness data in two-dimensional surface water models. Advances in Water Resources **34**(9), 1151–1164 (2011). DOI 10.1016/j.advwatres.2011.02.004
18. Jain, M.K., Kothyari, U.C., Ranga Raju, K.G.: A GIS based distributed rainfall–runoff model. Journal of Hydrology **299**(1-2), 107–135 (2004). DOI 10.1016/j.jhydrol.2004.04.024
19. Jain, M.K., Singh, V.P.: DEM-based modelling of surface runoff using diffusion wave equation. Journal of Hydrology **302**(1-4), 107–126 (2005). DOI 10.1016/j.jhydrol.2004.06.042
20. Lawrence, D.S.L.: Macroscale surface roughness and frictional resistance in overland flow. Earth Surface Processes and Landforms **22**, 365–382 (1997)
21. Liang, D., Falconer, R.A., Lin, B.: Coupling surface and subsurface flows in a depth averaged flood wave model. Journal of Hydrology **337**(1-2), 147–158 (2007). DOI 10.1016/j.jhydrol.2007.01.045
22. Liang, Q., Marche, F.: Numerical resolution of well-balanced shallow water equations with complex source terms. Advances in Water Resources **32**(6), 873–884 (2009). DOI 10.1016/j.advwatres.2009.02.010
23. McMillan, H.K., Brasington, J.: Reduced complexity strategies for modelling urban floodplain inunda-

tion. Geomorphology **90**(3-4), 226–243 (2007). DOI 10.1016/j.geomorph.2006.10.031

24. Morvan, H., Knight, D., Wright, N., Tang, X., Crossley, A.: The concept of roughness in fluvial hydraulics and its formulation in 1D, 2D and 3D numerical simulation models. Journal of Hydraulic Research **46**(2), 191–208 (2008). DOI 10.1080/00221686.2008.9521855
25. Mügler, C., Planchon, O., Patin, J., Weill, S., Silvera, N., Richard, P., Mouche, E.: Comparison of roughness models to simulate overland flow and tracer transport experiments under simulated rainfall at plot scale. Journal of Hydrology **402**(1-2), 25–40 (2011). DOI 10.1016/j.jhydrol.2011.02.032
26. Néelz, S., Pender, G.: Sub-grid scale parameterisation of 2D hydrodynamic models of inundation in the urban area. Acta Geophysica **56**(3), 65–72 (2007)
27. Razafison, U., Cordier, S., Delestre, O., Darboux, F., Lucas, C., James, F.: A Shallow Water model for the numerical simulation of overland flow on surfaces with ridges and furrows. European Journal of Mechanics - B/Fluids **31**, 44–52 (2012). DOI 10.1016/j.euromechflu.2011.07.002
28. Simons, F., Busse, T., Hou, J., Özgen, I., Hinkelmann, R.: A model for overland flow and associated processes within the Hydroinformatics Modelling System. Journal of Hydroinformatics **16**(2), 375–391 (2014). DOI 10.2166/hydro.2013.173
29. Smith, L.S., Liang, Q.: Towards a generalised GPU/CPU shallow-flow modelling tool. Computers & Fluids **88**, 334–343 (2013). DOI 10.1016/j.compfluid.2013.09.018
30. Smith, M.W.: Roughness in the Earth Sciences. Earth-Science Reviews **136**, 202–225 (2014). DOI 10.1016/j.earscirev.2014.05.016
31. Smith, M.W., Cox, N.J., Bracken, L.J.: Applying flow resistance equations to overland flows. Progress in Physical Geography **31**(4), 363–387 (2007). DOI 10.1177/0309133307081289
32. Souchere, V., King, D., Daroussin, J., Papy, F., Capillon, A.: Effects of tillage on runoff directions: consequences on runoff contributing area within agricultural catchments. Journal of Hydrology **206**(3-4), 256–267 (1998). DOI 10.1016/S0022-1694(98)00103-6
33. Stadler, L., Hinkelmann, R., Helmig, R.: Modeling macroporous soils with a two-phase dual-permeability model. Transport in Porous Media (95), 585–601 (2012)
34. Teuber, K., Özgen, I., Liang, D., Hinkelmann, R.: [Entwicklung eines Skalierungsansatzes zur Berücksichtigung von Mikrotopographie in den Flachwassergleichungen]. Unpublished.
35. Thompson, S.E., Katul, G.G., Porporato, A.: Role of microtopography in rainfall-runoff partitioning: An analysis using idealized geometry. Water Resources Research **46**(7) (2010). DOI 10.1029/2009WR008835
36. Toro, E.F., Spruce, M., Speares, W.: Restoration of the contact surface in the HLL-Riemann solver. Shock Waves **4**(1), 25–34 (1994). DOI 10.1007/BF01414629
37. Tsihrintzis, V.A., Wu, F.C., Shen, H.W., Chou, Y.J.: Discussion and Closure: Variation of Roughness Coefficients for Unsubmerged and Submerged Vegetation. Journal of Hydraulic Engineering **127**(3), 241–245 (2001)
38. Volp, N.D., van Prooijen, B.C., Stelling, G.S.: A finite volume approach for shallow water flow accounting for high-resolution bathymetry and roughness data. Water Resources Research **49**(7), 4126–4135 (2013). DOI 10.1002/wrcr.20324
39. van der Walt, S., Colbert, C.S., Varoquaux, G.: The NumPy array: A structure for efficient numerical compu-

tation. Computing in Science & Engineering **13**, 22–30 (2011)

40. Yörük, A.: Unsicherheiten bei der hydrodynamischen Modellierung von Überschwemmungsgebieten, *Mitteilungen / Institut für Wasserwesen*, vol. 99. Universität der Bundeswehr München (2009)
41. Yu, D., Lane, S.N.: Urban fluvial flood modelling using a two-dimensional diffusion-wave treatment, part 1: mesh resolution effects. Hydrological Processes **20**(7), 1541–1565 (2006). DOI 10.1002/hyp.5935
42. Zhu, C., Byrd, R.H., Nocedal, J.: L-BFGS-B: Algorithm 778: L-BFGS-B, FORTRAN routines for large scale bound constrained optimization. ACM Transactions on Mathematical Software **23**(4), 550–560 (1997)